The Physical Dipole Model and Polarizability for Magnetostatic Object Parameter Estimation

John S. Furey[1] and Dwain K. Butler[2]
[1]U.S. Army Engineer Research and Development Center, Environmental Laboratory, 3909 Halls Ferry Road, Vicksburg, Miss. 39180
Email: john.s.furey@usace.army.mil
[2]Applied Geophysics Consultancy LLC, 211 Grinders Place, Vicksburg, Miss. 39180

ABSTRACT

The physical dipole is the next simplest model of a magnetic object beyond the point dipole model. The theory and analytical properties of the physical dipole are developed and explored, and compare favorably with alternative models, including limiting cases of prolate spheroids and other shapes. The general applicability of explicitly modeling the demagnetization properties of magnetic materials is critically reviewed, and reasons proffered to use the object polarizability instead, especially for the external field properties of most relevance. Neither the physical dipole model nor polarizability is currently used for magnetostatic parameter estimation of magnetic objects such as unexploded ordnance. It is recommended that their utility be further explored with field data.

Introduction and Definitions

The magnetic field $\vec{\mathbf{B}}$ is affected by some materials more than others. The presence of objects made of magnetic materials distorts $\vec{\mathbf{B}}$ from what it would have been without the objects, and hence the spatial distribution of these anomalous distortions can be used to infer some aspects of the objects' locations, sizes, shapes, relative orientations, and material properties by inverse modeling of the measured magnetic field (Butler *et al.,* 2001). For magnetic detection of metal objects such as unexploded ordnance (UXO) in soil, such inference is done by parameter estimation relying on the fact that most soils are not very magnetic, and that many relevant metals, such as in UXO casings are ferrous and more magnetic than the surrounding soil (McFee, 1989). For soils with many natural anomalies, more detailed modeling of objects' properties, especially their shapes and materials, may enable better detection and discrimination from the natural background (Butler, 2003; Butler *et al.,* 2003).

Magnetic materials have magnetization $\vec{\mathbf{M}}$, and external to magnetic materials $\vec{\mathbf{M}}=0$. It is more convenient in magnetostatics when dealing with differing material properties to use the magnetizing field $\vec{\mathbf{H}}$ defined as $\vec{\mathbf{H}}\equiv\frac{1}{\mu_0}\vec{\mathbf{B}}-\vec{\mathbf{M}}$. The magnetic constant is $\mu_0\equiv 4\pi\times 10^{-7}\,\mathrm{T(A/m)^{-1}}$, where the units are tesla per (ampere per meter). The International System of units is used exclusively in this paper, and equations from references which use other parameterizations and notations are converted. The magnetic moment $\vec{\mathbf{m}}$ of an object caused by the object's magnetization is the integral $\vec{\mathbf{m}}\equiv\int \mathrm{dV}\,\vec{\mathbf{M}}$ over the volume V. For any (finite) magnetic object, $\vec{\mathbf{m}}$ is also the far-field dipole moment. The point dipole field $\vec{\mathbf{H}}_{\mathrm{DP}}$ is defined as:

$$\vec{\mathbf{H}}_{\mathrm{DP}}\equiv\frac{1}{4\pi}\frac{\mathrm{m}}{\mathrm{r}^3}[3(\hat{\mathrm{m}}\cdot\hat{\mathrm{r}})\hat{\mathrm{r}}-\hat{\mathrm{m}}]=\frac{1}{\mu_0}\vec{\mathbf{B}}_{\mathrm{DP}}, \qquad (1)$$

where $\vec{\mathbf{r}}\equiv\vec{\mathbf{x}}-\vec{\mathbf{x}}_0$ is the position $\vec{\mathbf{x}}$ relative to the location $\vec{\mathbf{x}}_0$ of the point dipole, and m is the magnitude of the point dipole moment. The directional quantity in square brackets in Eq. 1, comprising unit vectors denoted by carets, reaches its maximum magnitude of 2 along the axis of magnetization, and minimum magnitude of 1 perpendicular to the axis. The vector location and the vector dipole moment are the only parameters that can be estimated for the single point dipole.

The point dipole is by far the most commonly used model of the field produced by a magnetic object. Although it is inadequate for detailed modeling of effects of realistic UXO shapes, it is commonly and successfully used to determine equivalent object sizes and orientations, as well as locations and moments (McFee and Das, 1986; DeProspo and DiMarco, 1996; Barrow *et al.,* 1997; Altshuler *et al.,* 1997; Butler *et al.,* 1998; Nelson and McDonald, 1998; Billings, 2004; Gerovska *et al.,* 2004). By design, it provides adequate information in the far-field for estimation of the dipole moment and location, but it cannot by itself yield estimates of size, shape, relative orientation of object and field, and material

properties since these parameters are not in the model. Indeed, the point dipole model can even be inadequate for estimating the location of some relevant objects, especially giving ambiguous results when using data measured near the objects (Billings *et al.,* 2002).

Another kind of dipole is the so-called physical dipole. It comprises two coupled poles at a small distance L from each other. The location of the physical dipole is the center point, halfway between the two poles. An example of a manifestation of a magnetic physical dipole is a small segment of a Dirac string, which is essentially an infinitely narrow solenoid (Dirac, 1931). This manifestation avoids the need to introduce fictitious magnetic charges. A point directly on the Dirac string would be inside the singularity, but anywhere else the external field $\vec{\mathrm{H}}_{\mathrm{pd}}$ from a physical dipole of length L is defined to be:

$$\vec{\mathrm{H}}_{\mathrm{pd}} \equiv \frac{1}{4\pi}\frac{\mathrm{m}}{\mathrm{L}}\left[\frac{\mathrm{r}\,\hat{\mathrm{r}}-\frac{\mathrm{L}}{2}\hat{\mathrm{m}}}{\left|\mathrm{r}\,\hat{\mathrm{r}}-\frac{\mathrm{L}}{2}\hat{\mathrm{m}}\right|^{3}}-\frac{\mathrm{r}\,\hat{\mathrm{r}}+\frac{\mathrm{L}}{2}\hat{\mathrm{m}}}{\left|\mathrm{r}\,\hat{\mathrm{r}}+\frac{\mathrm{L}}{2}\hat{\mathrm{m}}\right|^{3}}\right]. \qquad (2)$$

In the far-field, *i.e.,* $\mathrm{r} \gg \frac{\mathrm{L}}{2}$, the series expansion of Eq. 2 approaches the point dipole as:

$$\vec{\mathrm{H}}_{\mathrm{pd}} = \frac{1}{4\pi}\frac{\mathrm{m}}{\mathrm{r}^3}\left[\left\{3(\hat{\mathrm{m}}\cdot\hat{\mathrm{r}})\,\hat{\mathrm{r}}-\hat{\mathrm{m}}\right\}+\frac{\mathrm{L}^2}{8\mathrm{r}^2}\left\{\left(-15(\hat{\mathrm{m}}\cdot\hat{\mathrm{r}})+35(\hat{\mathrm{m}}\cdot\hat{\mathrm{r}})^3\right)\hat{\mathrm{r}}-\left(-3+15(\hat{\mathrm{m}}\cdot\hat{\mathrm{r}})^2\right)\hat{\mathrm{m}}\right\}+\ldots\right].$$

The field of the physical dipole has azimuthal symmetry. With the z-axis the axis of symmetry, the easiest field component to calculate in Cartesian coordinates $\{\hat{\mathrm{x}},\hat{\mathrm{y}},\hat{z}\}$ is the z component H_z in the central plane perpendicular to the axis, where z = 0, and for this case the physical dipole field has the form:

$$\mathrm{H}_z = \frac{1}{4\pi}\frac{\mathrm{m}}{\mathrm{r}^3}\left[-\left(1+\frac{\mathrm{L}^2}{4\mathrm{r}^2}\right)^{-\frac{3}{2}}\right] = \frac{1}{4\pi}\frac{\mathrm{m}}{\mathrm{r}^3}\left[-1+\frac{3}{8}\frac{\mathrm{L}^2}{\mathrm{r}^2}-\frac{15}{128}\frac{\mathrm{L}^4}{\mathrm{r}^4}+\ldots\right]. \qquad (3)$$

After the point dipole, the physical dipole may be the next simplest model since it has only one more parameter: the length L. The physical dipole model has not been applied previously for magnetostatic parameter estimation of magnetic objects such as UXO. Many other models have been previously utilized for UXO detection and discrimination, including spheres, spheroids, and shells. The limiting case of a prolate spheroid as a magnetized splinter is examined herein as a potential candidate for another manifestation of the magnetic physical dipole.

The properties of the magnetized splinter are derived analytically as a limit of a prolate spheroid and compared with the physical dipole in a later section. Prior to that comparison, the general treatment of properties of the internal and external magnetostatic fields from objects is reviewed. Besides comparing with the physical dipole, in the context of UXO detection magnetic splinters are one common kind of scrap and it is appropriate to model their behavior in their own right, including low frequency and magnetostatic response (Bell and Barrow, 1997; Lieblich, 2004).

Sphere of Magnetic Material

There are no real point objects, but the external field from a perfect sphere of diameter D of uniform magnetization is exactly a point dipole with $\vec{\mathrm{m}} = \mathrm{V}\vec{\mathrm{M}} = \frac{\pi \mathrm{D}^3}{6}\vec{\mathrm{M}}$, and $\vec{\mathrm{H}} = -\frac{1}{3}\vec{\mathrm{M}}$ is the internal field from the magnetization of the uniform sphere (Reitz and Milford, 1962; Jackson, 1975). Two kinds of magnetization $\vec{\mathrm{M}}$ are remanent and induced. Remanent magnetization depends wholly upon the history of an object's material. Most intact UXO objects have negligible remanent magnetization compared to induced, although large ordnance fragments and shrapnel can have greater remanent magnetization than induced (Billings, 2009). In the context of object detection, magnetization is typically induced by an applied magnetizing field. That applied field is often simply the Earth's field, which is spatially quite uniform over the UXO range sizes relevant for detection of sub-meter size anomalies. Most ferrous UXO objects have magnetization that can be assumed to be mostly induced by and, for the most part, parallel to the local Earth's field (Altshuler, 1996).

Maxwell's equations entail linear superposition such that any additional uniform external applied field $\vec{\mathrm{H}}_{\mathrm{a}}$ induces an additional homogeneous internal field $\vec{\mathrm{H}}_1$. For a uniform sphere $\vec{\mathrm{H}}_1 = \vec{\mathrm{H}}_{\mathrm{a}} - \frac{1}{3}\vec{\mathrm{M}}_1$, where $\vec{\mathrm{M}}_1$ is the additional induced magnetization. Given a magnetic reference state $\vec{\mathrm{H}}_0$, $\vec{\mathrm{M}}_0$, which is often taken to represent zero field, then within sufficiently small changes in the induced fields $\vec{\mathrm{H}}_1 \equiv \vec{\mathrm{H}} - \vec{\mathrm{H}}_0$, $\vec{\mathrm{M}}_1 \equiv \vec{\mathrm{M}} - \vec{\mathrm{M}}_0$, a linearized constitutive relation can be used to define the susceptibility tensor χ for any material via $\vec{\mathrm{M}}_1 = \chi\vec{\mathrm{H}}_1$. For a magnetically isotropic material the susceptibility is a scalar proportional to the identity tensor 1, *i.e.,* $\chi = \chi\,1$, where χ is the scalar susceptibility. In that case, the induced magnetization in the material of a uniform isotropic sphere is given by $\vec{\mathrm{M}}_1 = \frac{\chi}{1+\frac{1}{3}\chi}\vec{\mathrm{H}}_{\mathrm{a}}$. Then the external induced field, given by Eq. 1 with $\mathrm{m} = \frac{\pi \mathrm{D}^3}{6}\mathrm{M}_1$, can have a magnitude that exceeds the magnitude of the applied field near the sphere, provided $\chi > 3$. Most

materials have either a very small positive $\chi \ll 1$ (paramagnetic), large positive $\chi \gg 1$ (strongly magnetic, *e.g.,* ferromagnetic), or very small negative χ (diamagnetic). Many parameterizations of magnetic models alternatively use the relative permeability μ_r defined as $\mu_r \equiv \chi + 1$.

By definition, the susceptibility is a material parameter that can be best estimated directly by varying the applied field, although in the context of object detection the possible material susceptibilities are already in known model libraries. Magnetic measurements can then serve to indirectly estimate χ in several broad categories. For example, the ferrous materials used in UXO and landmines typically have measured susceptibilities in the range 100–1,000 (Won *et al.,* 2001; Billings *et al.,* 2006). Hence, given other details about a magnetic object, some material susceptibility discrimination is possible even in a constant applied field such as the Earth's field.

Other Parameters of Magnetic Spheres

As an example of using material discrimination, if the magnitude of the induced field measured near a spherical object is greater than or even a significant fraction of the applied field, then the material must have large positive χ and hence it is undoubtedly ferrous. Then for an unsaturated ferrous sphere in a small applied field, the measurement of the induced dipole moment m enables inference of the size (volume V) of the sphere because $M_1 \approx 3H_a$ so:

$$V \approx \frac{m}{3H_a}. \tag{4}$$

Although Eq. 4 is not often directly applied, similar empirical correlations allow estimation of ferrous volume for specific UXO types (Pennella, 1982).

In all strongly magnetic materials not only is the susceptibility large in small applied fields, but the magnetization saturates at the material-specific value M_{sat} in large fields. Any remanent magnetization for UXO will be below the saturation value, but in laboratory experiments with ferrous materials the magnetization is often saturated or near saturation.

Strongly magnetic materials also tend to exhibit hysteresis, in which the field required to produce a particular magnetization depends upon the history. The dual phenomena of saturation and hysteresis preclude a linear constitutive relation for all strongly magnetic materials. An example of a simple nonlinear constitutive relation is $\vec{M}_1 = \left(1 - \frac{M}{M_{sat}}\right)\chi \vec{H}_1$, where χ depends upon the magnetic reference state and hence can be history dependent.

If the applied field can be varied enough to produce saturation, then the saturation magnetization is another material parameter that can be directly estimated *e.g.,* by sequentially increasing magnetic field measurements. Otherwise, like the susceptibility it can be indirectly estimated through a material library. It is important to keep in mind that ferrous objects may have some remanent magnetization, and vice versa that the presence of any significant remanent magnetization requires strongly magnetic material. With or without remanent magnetization, the external fields produced by the magnetization of a uniform sphere are still purely dipolar, even fields at or above saturation.

Non-spherical Objects

Most objects are not spheres, and many intact UXO are quite elongated and roughly cylindrically symmetric (*e.g.,* Butler *et al.,* 2002; Billings, 2004). Many other objects of interest in UXO ranges are metal splinters, bits of wire, fragments of tailfins, shards of casing material, and other shrapnel (*e.g.,* Lieblich, 2004; Billings, 2009), none very spherical in shape at all. The magnetic field distortions from these nonspherical objects are not purely dipole, and near the objects the field measurements provide information that can enable estimates of their shapes and orientations (Billings *et al.,* 2006).

Because an object's magnetic field is stronger nearer the object, the data collected near an object tends to be of higher signal-to-noise ratio than the data collected in the far-field. However, for a nonspherical object the use of the nominally better near-field data to help estimate parameters of an incompatible model, namely the far-field point dipole, can actually lead to worse results. Of course, overlapping fields from nearby objects can also produce nondipolar fields, but the problems of estimating with a number of multiple objects are different than the problems of estimating properties of single objects (Rene *et al.,* 2008). Attempts have been made to approximately model object shape effects in other ways, such as with combinations of dipoles (Sun *et al.,* 2006), but correctly calculating the magnetostatic properties of a nonspherical object relies on application of magnetic potential boundary value analyses.

Magnetic Potential

The magnetostatic Maxwell's equations imply the existence of the pseudoscalar magnetic potential Φ, where $\vec{B} = -\frac{\mu_0}{4\pi}\nabla\Phi$, obeying Laplace's equation $\nabla^2\Phi = 0$ external to magnetic material. This external potential can be expressed in the usual multipole expansion (Kellogg, 1954) as:

$$\Phi = \frac{\vec{m}\cdot\vec{r}}{r^3} + \frac{1}{2}\frac{(\mathbf{Q}\,\vec{r})\cdot\vec{r}}{r^5} + \ \ldots, \tag{5}$$

where **Q** is the quadrupole moment tensor. The monopole term is identically zero for magnetic fields. The contribution of higher order multipole moments to the external fields falls off rapidly with distance.

Parameter estimation of a general object shape from measurements of external fields typically involves comparison of the relative strengths of components of the multipole moments through fitting to fields derived from Eq. 5, with appropriate matching of values and derivatives at boundaries between materials. For many UXO items, the octupole moments may provide the best shape discrimination (Butler, 2001).

Internal Fields of General Objects

To account for shape effects on internal fields of objects, it is customary to define the demagnetization tensor **N** such that the internal field induced by an applied field $\vec{\mathbf{H}}_a$ is:

$$\vec{\mathbf{H}}_1 = \vec{\mathbf{H}}_a - \mathbf{N}\vec{\mathbf{M}}_1. \tag{6}$$

It should be cautioned that Eq. 6 is not a fundamental relation, but instead defines **N**. Note that for a uniform sphere, **N** is the scalar $\frac{1}{3}1$. In general, Eq. 6 as written is a local relation for the point function **N**. For uniform magnetization, the point function demagnetization tensor has an expression that only depends on the shape of the boundary and obeys trace(**N**) = 1 for any shape (Schlomann, 1962). However, for inhomogeneous magnetization trace(**N**) $\neq$ 1, and Eq. 6 is not useful as a point function relation as further detailed below.

For any linear constitutive relation, by inspection of Eq. 6 the induced field $\vec{\mathbf{H}}_1 = (1+\mathbf{N}\boldsymbol{\chi})^{-1}\vec{\mathbf{H}}_a$ and the induced magnetization:

$$\vec{\mathbf{M}}_1 = \boldsymbol{\chi}(1+\mathbf{N}\boldsymbol{\chi})^{-1}\vec{\mathbf{H}}_a \tag{7}$$

are clearly homogeneous for a homogenous $\boldsymbol{\chi}$ if and only if **N** is also homogenous. The same conclusion also holds for any nonlinear constitutive relation (Brown, 1962; Cape and Zimmerman, 1967). In general, **N** as defined in Eq. 6 can even depend on the fields and materials as well as shapes. For a general shape and material, to obtain the internal fields there is no analytical alternative to working through the full boundary value problem numerically, and Eq. 6 provides no analytical help when **N** varies with position inside the object. Despite that fact, many lists of operationally defined averaged effective demagnetization factors for objects with other shapes have been published, which have utility within their application (*e.g.,* Stoner, 1945; Moskowitz *et al.,* 1966; Chen *et al.,* 1991; Pardo *et al.,* 2004, Chen *et al.,* 2005; Gorkunov *et al.,* 2005).

Magnetometric demagnetization. The volume averaged point function demagnetization tensor of an object, denoted here by $\langle\mathbf{N}\rangle$ and defined via $V\langle\mathbf{N}\rangle \equiv \int dV\,\mathbf{N}$, is often called the magnetometric demagnetization tensor and it obeys trace($\langle\mathbf{N}\rangle$) = 1 for uniform magnetization (Moskowitz and Della Torre, 1966). The volume averaged demagnetization tensor or its effective equivalent is often inexactly utilized for nonuniform magnetization for both the discretized (Schabes and Aharoni, 1987) and continuum (Newell *et al.,* 1993) cases. But as written for the point function demagnetization, Eq. 6 does not decouple into volume averages: $\langle\vec{\mathbf{H}}_1\rangle \neq \langle\vec{\mathbf{H}}_a\rangle - \langle\mathbf{N}\rangle\langle\vec{\mathbf{M}}_1\rangle$. The reason is because $\langle\mathbf{N}\vec{\mathbf{M}}_1\rangle \neq \langle\mathbf{N}\rangle\langle\vec{\mathbf{M}}_1\rangle$. The difference between the average of the product and the product of the averages is the covariance, which does not vanish in general.

In fact, the magnetometric demagnetization tensor of an object, denoted here by $\overline{\mathbf{N}}$, is experimentally defined in terms of its effect on the ratios of volume averages of fields as $\overline{\mathbf{N}}\langle\vec{\mathbf{M}}_1\rangle \equiv \langle\vec{\mathbf{H}}_a - \vec{\mathbf{H}}_1\rangle$ (Zijlstra, 1967). Hence, in general, this experimental magnetometric demagnetization tensor is not equal to the volume averaged point function demagnetization tensor. And in actual practice when performing magnetometric measurements on an object, the volume averaging is not even performed as indicated (*e.g.,* by averaging measurements of the internal fields and magnetization at many different points inside the object). Instead, the average is operationally defined by its overall effect on external fields, *i.e.,* deduced from magnetometer measurements of the external fields at multiple external points.

To isolate the overall effects of any specific shape, the experimental procedure is to utilize materials with well characterized constitutive relations. Because by definition the induced dipole moment of the object is $\vec{\mathbf{m}}_1 = V\langle\vec{\mathbf{M}}_1\rangle$, the dipole moment and other fitted parameters (such as higher moments) of the measured external fields can be used to infer components of the magnetometric demagnetization tensor. Models can then predict the unmeasured internal fields if the internal fields are needed. However, in the context of UXO detection, the internal fields are not themselves needed; their relevance is their effects on external fields.

Object polarizability. Instead of using internal object parameters such as demagnetization, external object parameters can be used, specifically the object polarizability tensor $\boldsymbol{\alpha}$ defined as $\vec{\mathbf{m}}_1 \equiv \boldsymbol{\alpha}\vec{\mathbf{H}}_a$. For example, for a linear constitutive relation, Eq. 7 shows that the polarizability obeys $\boldsymbol{\alpha} = V\langle\boldsymbol{\chi}(1+\mathbf{N}\boldsymbol{\chi})^{-1}\rangle$, and in terms of the magnetometric demagnetization rigorously:

$$\boldsymbol{\alpha} = V\,\boldsymbol{\chi}\left(1+\overline{\mathbf{N}}\,\boldsymbol{\chi}\right)^{-1} \tag{8}$$

for homogenous linear $\boldsymbol{\chi}$. In practice, for any given constitutive relation the estimation of $\boldsymbol{\alpha}$ can instead be

used to calculate the magnetometric demagnetization if needed, for instance by $\overline{\mathbf{N}} = \mathrm{V}\boldsymbol{\alpha}^{-1} - \boldsymbol{\chi}^{-1}$.

In classical electromagnetism, for a homogeneous material the object polarizability is always directly proportional to the object volume, as in Eq. 8, which permits a good estimate of the volume similar to Eq. 4. In addition the polarizability formalism is directly extendible to higher order multipoles along with external field gradients, and to nonlinear terms called hyperpolarizabilies (Mahan and Subbaswamy, 1990), most often used in high frequency models of atomic response. Although the magnetostatic polarizability is not currently used as such in magnetostatic UXO detection models, models with frequency dependent polarizability parameters are often utilized in low frequency electromagnetic induction detection of UXO (Norton *et al.,* 2001; Smith and Morrison, 2004; Gasperikova *et al.,* 2007; Shubitidze *et al.,* 2007; Billings *et al.,* 2008).

Internal Fields of Prolate Spheroids

Because Laplace's equation is a second order partial differential equation, the internal induced field and magnetization of an object are homogeneous if and only if the boundary (the object's surface) is specified by a quadratic form (Maxwell, 1891). Therefore, to be able to use a single point function demagnetization tensor, the object's material must be homogenous and the object's surface must be specified by a quadratic form. For all other cases, the point function **N** varies with position inside the object. The most general quadratic form is an ellipsoid, and **N** is diagonal when transformed into the principal axes coordinates of the ellipsoid. Each of these diagonal entries is called the demagnetization factor for that axis.

The demagnetization factors of the general ellipsoid have been worked out analytically using potential theory with a linear constitutive relation (Osborn, 1945). For a scalene ellipsoid, the demagnetization factors are given in terms of combinations of incomplete elliptic integrals. For ellipsoids of revolution, *i.e.,* spheroids, the demagnetization factors are elementary functions of the aspect ratio γ, defined to be the ratio of the length L of the object (along the axis of symmetry) to the diameter D of the object (perpendicular to the axis of symmetry). For spheroids, the object volume is: $\mathrm{V} = \frac{\pi \mathrm{D}^3}{6}\gamma = \frac{\pi \mathrm{L}^3}{6\gamma^2}$.

To keep things straight, it is most convenient to use Cartesian coordinates $\{\hat{\mathrm{x}}, \hat{\mathrm{y}}, \hat{\mathrm{z}}\}$, with **N** diagonal. $\mathrm{N_{zz}}$ is the factor along the axis of symmetry and $\mathrm{N_{xx}}$ in any one particular direction perpendicular to the axis of symmetry. For a prolate spheroid ($\gamma > 1$):

$$\mathrm{N_{xx}} = \mathrm{N_{yy}} = \frac{1 - \mathrm{N_{zz}}}{2},\ \mathrm{N_{zz}} = \frac{\frac{\gamma}{\sqrt{\gamma^2 - 1}}\operatorname{acosh}(\gamma) - 1}{\gamma^2 - 1}, \qquad (9)$$

where acosh is the inverse hyperbolic cosine.

Some special limiting cases are of interest. For the prolate spheroid, the magnetized splinter (line segment) has a vanishing D with a fixed length L = D γ, and the long rod (infinitely long cylinder) has fixed D with divergent length L. To leading order of the expansions of Eq. 9 in terms of aspect ratio for the splinter and long rod, $\mathrm{N_{zz}} = 0$, $\mathrm{N_{xx}} = \mathrm{N_{yy}} = \frac{1}{2}$, and $\mathrm{N_{zz}}$ vanishes as $\mathrm{N_{zz}} \to \frac{\ln(\gamma)}{\gamma^2}$. For a linear isotropic constitutive relation, the components of magnetization induced by $\vec{\mathbf{H}}$ are $\mathrm{M_x} = \frac{\chi}{1 + \mathrm{N_{xx}}\chi}\mathrm{H_x}$, $\mathrm{M_y} = \frac{\chi}{1 + \mathrm{N_{yy}}\chi}\mathrm{H_y}$, $\mathrm{M_z} = \frac{\chi}{1 + \mathrm{N_{zz}}\chi}\mathrm{H_z}$. Therefore for very large susceptibility the induced magnetization for a prolate spheroid will tend to be along the z-axis, *i.e.,* the dimension of the object with the longest stretch of magnetic material, which necessarily has the smallest demagnetization factor. These considerations illuminate the general situation in which both **N** and $\vec{\mathbf{M}}$ are inhomogeneous; since changing the one changes the other, they will generally have a nonvanishing covariance.

Demagnetization tensor of oblate spheroids. For comparison and completeness, the limiting case of an oblate spheroid ($\gamma < 1$), *i.e.,* the circular shard or disk, has vanishing thickness L = D γ with a fixed D, and the slab (infinitely extensive layer) has a fixed thickness L with divergent D. For an oblate spheroid the expressions for the demagnetization factors are:

$$\mathrm{N_{xx}} = \mathrm{N_{yy}} = \frac{1 - \mathrm{N_{zz}}}{2},\ \mathrm{N_{zz}} = \frac{\frac{\gamma}{\sqrt{1 - \gamma^2}}\operatorname{acos}(\gamma) - 1}{\gamma^2 - 1}.$$

To leading order of these expressions in terms of the aspect ratio for the shard and slab, $\mathrm{N_{zz}} = 1$, $\mathrm{N_{xx}} = \mathrm{N_{yy}} = 0$, and $\mathrm{N_{xx}}$ vanishes as $\mathrm{N_{xx}} \to \frac{\pi}{4}\gamma$. Oblate spheroids have found use in modeling some plate-like objects, but are not further discussed herein since they have no direct bearing on the splinter analysis and physical dipole model.

Polarizability tensor of prolate spheroids. Because the internal induced fields and magnetization of spheroids are all uniform, the volume averaged point function demagnetization tensor and the magnetometric demagnetization tensor are also uniform, and therefore the same as the point function demagnetization tensor. The polarizability $\boldsymbol{\alpha}$ is diagonal, and for a linear isotropic constitutive relation its components are:

$$\alpha_{\mathrm{xx}} = \alpha_{\mathrm{yy}} = \frac{\mathrm{V}\chi}{1 + \frac{\chi}{2} - \frac{\chi}{2}\mathrm{N_{zz}}},\ \alpha_{\mathrm{zz}} = \frac{\mathrm{V}\chi}{1 + \chi\,\mathrm{N_{zz}}},$$

where $\mathrm{N_{zz}}$ is given in Eq. 9.

For the magnetized splinter, the dipole moment $\vec{\mathbf{m}}$ is given and the internal fields are not of interest, one major reason being the vanishing volume. Given $\vec{\mathbf{m}}$ the

polarizability is still defined, however, and if desired the magnetized splinter can be modeled as having a very small $V \ll L^3$ of magnetic material with very large $\chi \gg 1$. Then, for the magnetized splinter in that limit:

$$\alpha_{xx} = \alpha_{yy} = V2,\ \alpha_{zz} = V\chi. \tag{10}$$

The volume diverges for the infinitely long rod, and hence the dipole moment and polarizability diverge for any real magnetic material. However, if the long rod can be modeled as having very large $V \gg D^3$ and very small $\chi \ll 1$, then for the long rod in that limit:

$$\alpha_{xx} = \alpha_{yy} = \alpha_{zz} = V\chi.$$

External Fields of Prolate Spheroids

The external fields of the homogeneously magnetized general ellipsoid have been worked out analytically, and do not involve any specific constitutive relation (Tejedor *et al.,* 1995). For scalene ellipsoids, the external fields are given in terms of combinations of incomplete elliptic integrals. For spheroids, the z-axis is taken to be the axis of symmetry. For the prolate spheroid, following Tejedor *et al.* (1995) it is convenient to define the focal distance f by $2f \equiv D\sqrt{\gamma^2-1} = L\frac{\sqrt{\gamma^2-1}}{\gamma}$, and the auxiliary variables A and w by $A^2 = \sqrt{\left(r^2+f^2\right)^2 - 4z^2f^2}$ and $2f^2w^2 = \left(r^2+f^2\right) + A^2$. The contribution to the external magnetic field from the component of the magnetization M_z along the z-axis retains azimuthal symmetry and in Cartesian coordinates it is:

$$\begin{aligned} H_x &= \frac{1}{4\pi} m_z \frac{3}{f^3}\left[\frac{z\,x}{w(w^2-1)A^2}\right], \\ H_y &= \frac{1}{4\pi} m_z \frac{3}{f^3}\left[\frac{z\,y}{w(w^2-1)A^2}\right], \\ H_z &= \frac{1}{4\pi} m_z \frac{3}{f^3}\left[-\operatorname{acoth}(w) + \frac{1}{w} + \frac{z^2}{w^3A^2}\right], \end{aligned} \tag{11}$$

where acoth is the inverse hyperbolic cotangent. Note $\vec{m} = V\vec{M} = \frac{\pi L^3}{6\gamma^2}\vec{M}$. The contribution to the external magnetic field from the magnetization M_x in any particular direction perpendicular to the z-axis breaks azimuthal symmetry and in Cartesian coordinates it is:

$$\begin{aligned} H_x &= \frac{1}{4\pi} m_x \frac{3}{f^3}\left[\frac{\operatorname{acoth}(w)}{2} - \frac{w}{2(w^2-1)} + \frac{x^2w}{2(w^2-1)^2A^2}\right], \\ H_y &= \frac{1}{4\pi} m_x \frac{3}{f^3}\left[\frac{y\,x\,w}{(w^2-1)^2A^2}\right], \\ H_z &= \frac{1}{4\pi} m_x \frac{3}{f^3}\left[\frac{z\,x}{w(w^2-1)A^2}\right]. \end{aligned} \tag{12}$$

The case of general magnetization is found by linear combination of Eqs. 11 and 12, along with orientation of the axes. The parameters to be estimated for spheroids are primarily overall shapes and the relative orientation of the principal axes to the magnetization (Billings *et al.,* 2002), as well as the parameters previously discussed for spheres (*i.e.,* location and dipole moment, and some aspects of size and material).

Because the fields have been worked out, direct fits of their functional forms can produce direct estimates of parameters for spheroids, but the complicated parameterization results in difficult model inversion. Multipole fits can also be performed for these spheroids and are more robust and effective because of the smaller number of adjustable parameters, but still suffer from ambiguous model inversion (Billings *et al.,* 2002).

Fields of Spheroidal Shells

Because the ferrous material of many UXO objects is primarily in the outer shell casings, the thickness of such a shell was considered as an additional parameter to fit in a more realistic model. The internal and external fields of general confocal spheroidal shells have been worked out analytically with a strictly linear isotropic constitutive relation, in terms of linear combinations of associated Legendre functions in spheroidal coordinates (Frumkis and Kaplan, 1999). In these shells, the homogeneous magnetic material is confined between inner and outer confocal spheroidal boundaries, and the interior of the inner spheroid is a cavity. The internal fields in the material vary, and then the demagnetization tensor is not at all useful but can be calculated from its definition in Eq. 6. The special case of the spherical shell is worked out here.

Internal Fields of Spherical Shells

The spherical shell with linear isotropic χ is a textbook example (Jackson, 1975), although the resulting demagnetization tensor has not been exhibited previously. Following Jackson (1975) inside the magnetic material between radii a and b the components of the internal induced magnetizing field from an applied field $\vec{H}_a = H_a\,\hat{z}$ are:

$$\begin{aligned} H_x &= \frac{3\,\delta\,z\,x}{r^5}H_a,\ H_y = \frac{3\,\delta\,z\,y}{r^5}H_a, \\ H_z &= \left(\frac{3\,\delta\,z^2}{r^5} - \beta - \frac{\delta}{r^3}\right)H_a, \end{aligned}$$

where the coefficients β and δ are unfortunately complicated. Explicitly

$$\beta = -\frac{\left(3+\frac{11}{2}\frac{a^3}{b^3}\right)\chi+\left(3+\frac{9}{2}\frac{a^3}{b^3}\right)}{\left[(\chi+1)(\chi+3)-\frac{a^3}{b^3}\chi^2\right]\left(1-\frac{a^3}{b^3}\right)},$$

$$\delta = \frac{\left(-\frac{3}{2}+10\frac{a^3}{b^3}\right)\chi+\left(-\frac{3}{2}+9\frac{a^3}{b^3}\right)}{\left[(\chi+1)(\chi+3)-\frac{a^3}{b^3}\chi^2\right]\left(1-\frac{a^3}{b^3}\right)}a^3$$

Because the internal field varies and $H_x \neq 0$, $H_y \neq 0$, then $\mathbf{N}$ is inhomogeneous and nondiagonal.

$$\text{With } \mathbf{N} = \begin{bmatrix} N_{xx} & N_{xy} & N_{yz} \\ N_{yx} & N_{yy} & N_{yz} \\ N_{zx} & N_{zy} & N_{zz} \end{bmatrix} \text{ and for } \delta \neq 0,$$

$$N_{xy} = N_{yx} = \frac{3xy}{\chi r^2},\ N_{xz} = N_{zx} = \frac{3xz}{\chi r^2},\ N_{zy} = N_{yz} = \frac{3zy}{\chi r^2},$$

$$N_{xx} = \frac{3x^2}{\chi r^2} - \frac{3}{\chi} + \frac{\beta r^3}{\chi \delta},\ N_{yy} = \frac{3y^2}{\chi r^2} - \frac{3}{\chi} + \frac{\beta r^3}{\chi \delta},$$

$$N_{zz} = \frac{3z^2}{\chi r^2} - \frac{3}{\chi} - \frac{r^3}{\chi \delta}\frac{1-2\beta+3\beta\frac{z^2}{r^2}-2\frac{\delta}{r^3}}{1+\beta\frac{r^3}{\delta}-3\frac{z^2}{r^2}},$$

which can be laboriously verified by substitution in its defining Eq. 6. As remarked earlier, this does not obey trace($\mathbf{N}$) = 1, and this point function demagnetization tensor does not appear useful.

Polarizability Tensor of Spherical Shells

The volume averages of the components of the internal fields are given by:

$$\langle H_x \rangle = 0,\ \langle H_y \rangle = 0,\ \langle H_z \rangle = -\beta H_a.$$

Similarly,

$$\langle M_x \rangle = 0,\ \langle M_y \rangle = 0,\ \langle M_z \rangle = -\chi \beta H_a.$$

The volume-averaged point function demagnetization tensor $\langle \mathbf{N} \rangle$ is diagonal with:

$$\langle N_{xx} \rangle = \langle N_{yy} \rangle = -\frac{2}{\chi} + \frac{\beta}{\chi\delta}\frac{b^3+a^3}{2},$$

$$\langle N_{zz} \rangle = \frac{-1-5\beta}{\chi\beta} + \frac{\delta}{\chi\beta(b^3-a^3)}$$

$$\int_0^1 dc\left(-1+12c^2-9c^4+5+\frac{1}{\beta}\right)\ln\left|\frac{1+\beta\frac{b^3}{\delta}-3c^2}{1+\beta\frac{a^3}{\delta}-3c^2}\right|.$$

This does not obey trace $(\langle \mathbf{N} \rangle) = 1$, and it also does not appear useful. The covariance of $\mathbf{N}$ and $\vec{\mathbf{M}}$ is $\langle \mathbf{N}\vec{\mathbf{M}}_1 \rangle - \langle \mathbf{N} \rangle \langle \vec{\mathbf{M}}_1 \rangle$, which has a nonvanishing z component. Moreover, despite the overall spherical symmetry of the spherical shell, these volume-averaged point function demagnetization factors are not all equal.

In contrast, from its definition the magnetometric demagnetization tensor $\overline{\mathbf{N}}$ is diagonal and all of the magnetometric demagnetization factors are equal:

$$\overline{N}_{xx} = \overline{N}_{yy} = \overline{N}_{zz} = -\frac{1}{\chi} - \frac{1}{\chi\beta},$$

although it does not obey trace $(\overline{\mathbf{N}}) = 1$. It should be clear that $\overline{\mathbf{N}}$ is not the same as $\langle \mathbf{N} \rangle$. The previously mentioned covariance is easiest to calculate using the relation $\langle \mathbf{N}\vec{\mathbf{M}}_1 \rangle - \langle \mathbf{N} \rangle \langle \vec{\mathbf{M}}_1 \rangle = \overline{\mathbf{N}} \langle \vec{\mathbf{M}}_1 \rangle - \langle \overline{\mathbf{N}} \rangle \langle \vec{\mathbf{M}}_1 \rangle$. Therefore, the difference $\overline{\mathbf{N}} - \langle \mathbf{N} \rangle$ is of direct importance and can be called the demagnetization covariance tensor of the object.

The polarizability $\boldsymbol{\alpha}$ of the spherical shell is diagonal with equal factors:

$$\alpha_{xx} = \alpha_{yy} = \alpha_{zz} = -\frac{4}{3}\pi(b^3-a^3)\,\chi\,\beta.$$

External Fields of Spheroidal Shells

In contrast to the internal fields, the external fields and dipole moment of spheroidal shells, even for fairly thin shells, turn out to be approximately the same as those of a single filled spheroid, *i.e.,* without a cavity, completely filling the outer boundary surface (Altshuler, 1996; Butler *et al.,* 2004; Herrera-May *et al.,* 2009). For example, inserting values for the spherical shell shows that its polarizability actually depends mostly on the outer volume as:

$$\alpha_{xx} = \alpha_{yy} = \alpha_{zz} = \frac{4}{3}\pi b^3 \chi \frac{\left(3+\frac{11}{2}\frac{a^3}{b^3}\right)\chi+\left(3+\frac{9}{2}\frac{a^3}{b^3}\right)}{\left[(\chi+1)(\chi+3)-\frac{a^3}{b^3}\chi^2\right]},$$

with relatively minor dependence on the shell thickness.

At least for spheroidal objects, it is thus the outer volume of magnetic material that matters most for external fields, not the ferrous mass or actual thickness of magnetic material. Attempting to estimate minor parameters such as the thickness of the shell merely makes the parameter fitting more complicated and hence subject to greater error in other fitted parameters. Similar conclusions are expected to hold for other shapes as well.

Comparisons with the Physical Dipole

The external fields of the limiting prolate spheroid will now be compared with the physical dipole. The magnetized splinter is obtained in the limit as D vanishes, keeping L and $\vec{\mathbf{m}}$ fixed. For the magnetized splinter, the object orientation is fixed by $\vec{\mathbf{m}}$ and the field from the magnetization is azimuthally symmetric, as

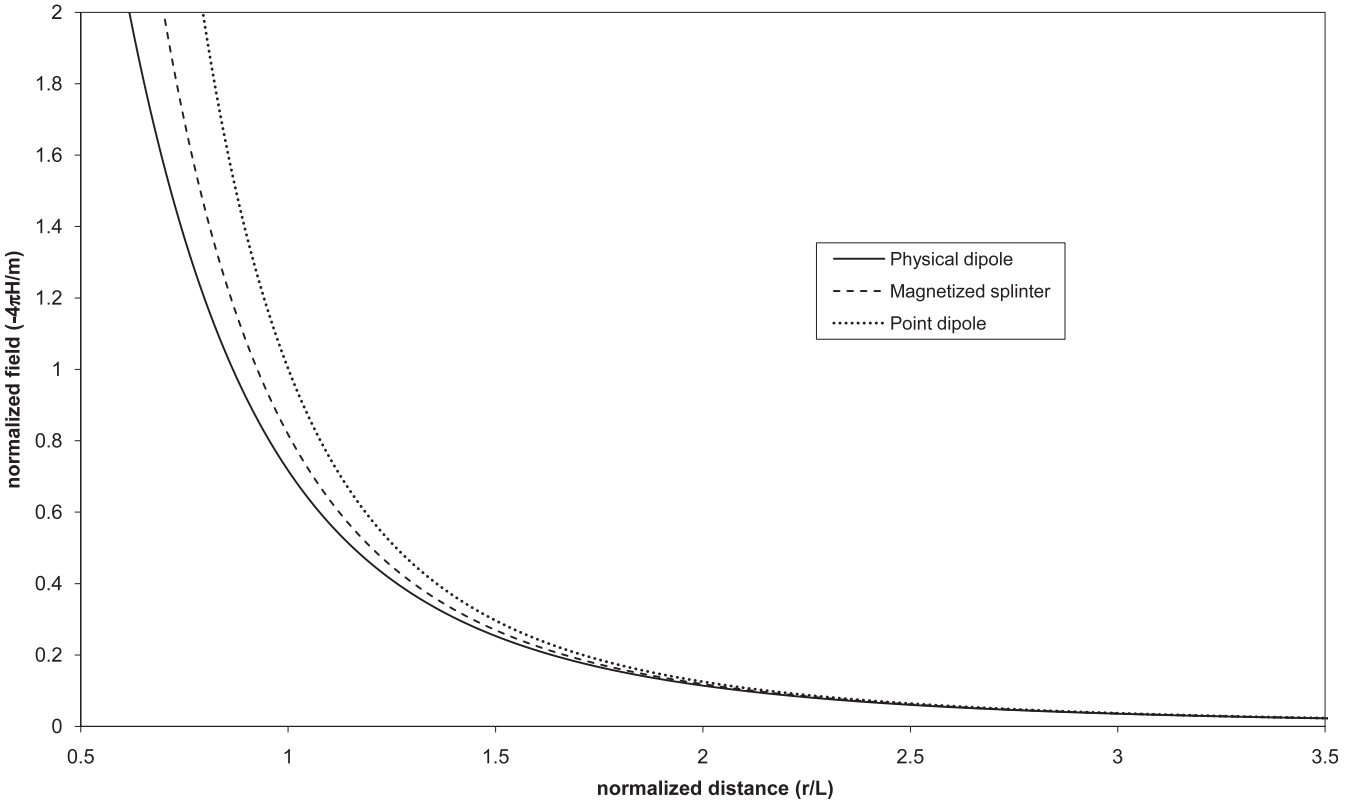

Figure 1. Comparison of normalized cross-axis fields for dipole models. The field strength of the magnetized splinter is between the physical dipole and the point dipole.

with the physical dipole. Although in the limit the volume vanishes, because $2f = L$ all of the quantities in Eq. 9 are well behaved.

Strengths of External Field

The easiest field component to calculate for the magnetized splinter is the z component in the central plane perpendicular to the axis, where $z = 0$, and for this case:

$$H_z = \frac{1}{4\pi}\frac{24\,m}{L^3}\left[-\operatorname{acoth}\left(\sqrt{\frac{4r^2}{L^2}+1}\right)+\frac{1}{\sqrt{\frac{4r^2}{L^2}+1}}\right]$$

$$= \frac{1}{4\pi}\frac{m}{r^3}\left[-1+\frac{7}{40}\frac{L^2}{r^2}-\frac{3}{128}\frac{L^4}{r^4}+\ldots\right]. \qquad (13)$$

Clearly the series expansion of this case, the cross-axis magnetized splinter in Eq. 13, is not the same as the expansion for the physical dipole in Eq. 3, although it can be shown that the signs of all the terms are the same. Indeed, the magnetized splinter is not an exact representation of the physical dipole. However their expressions allow easy comparison in both the near field and far field, along with the point dipole.

The strength of the cross-axis fields of the point dipole (magnetized sphere), magnetized splinter, and physical dipole are plotted in Fig. 1. The fields are normalized to the strength of the point dipole being 1 at $r = 1$, and the distances are normalized to $L = 1$. Both the magnetized splinter and physical dipole are somewhat weaker than the point dipole. If using the point dipole approximation to fit their measured data, these objects could be predicted to be somewhat farther than they really are. The field from the magnetized splinter is intermediate between the sphere and the physical dipole.

The next easiest case to compare is on-axis, where $x = y = 0$, and the field is in the positive z direction. For the physical dipole this on-axis field is:

$$H_z = \frac{1}{4\pi}\frac{m}{r^3}\left[\frac{r}{L}\left(1-\frac{L}{2r}\right)^{-2}-\frac{r}{L}\left(1+\frac{L}{2r}\right)^{-2}\right]$$

$$= \frac{1}{4\pi}\frac{m}{r^3}\left[2+\frac{L^2}{r^2}+\frac{3}{8}\frac{L^4}{r^4}+\ldots\right].$$

For the magnetized splinter the on-axis external field results from using $A^2 = \left|r^2 - \frac{L^2}{4}\right|$, so therefore $w = 2\frac{r}{L}$ for $r > \frac{L}{2}$. Note the singularity caused by $w = 1$ for $r \le \frac{L}{2}$. The on-axis external field is:

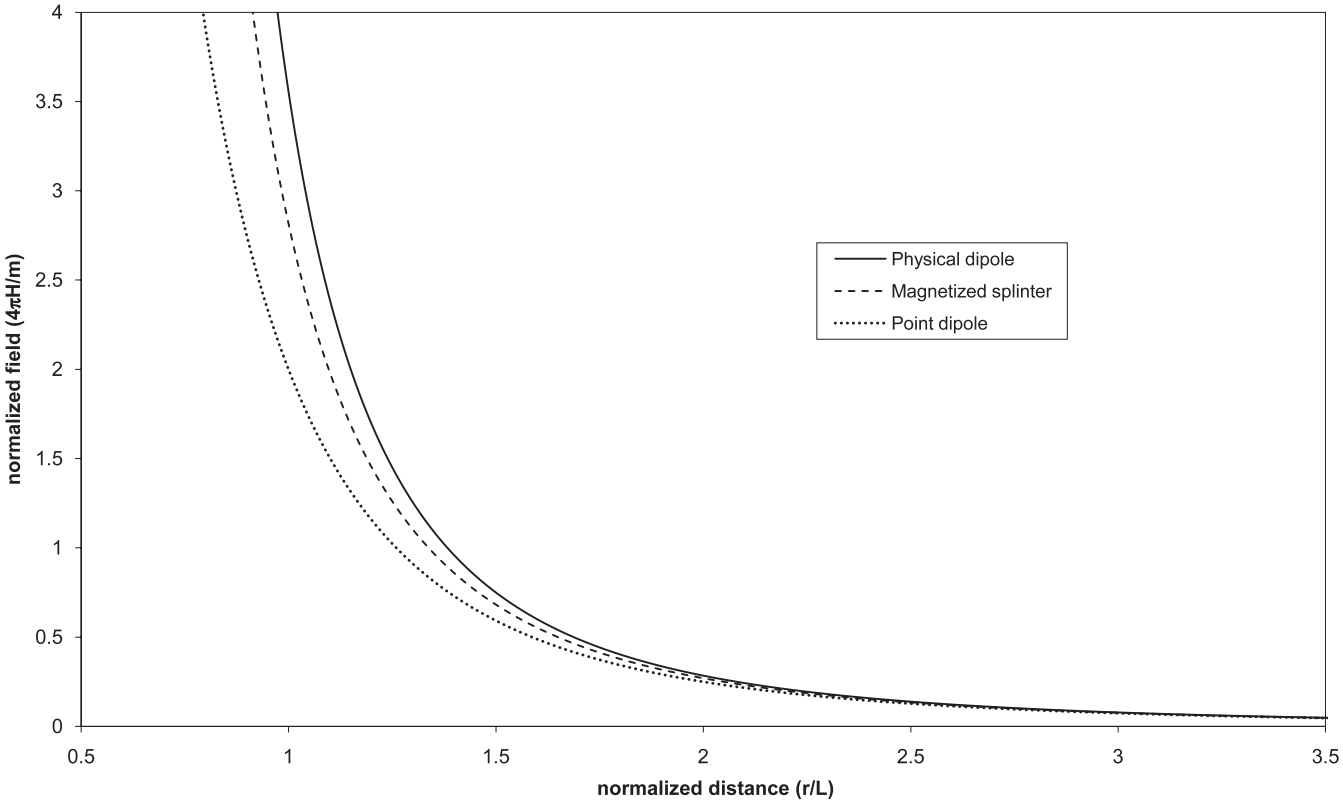

Figure 2. Comparison of normalized on-axis fields for dipole models. The field strength of the magnetized splinter is between the physical dipole and the point dipole.

$$H_z = \frac{1}{4\pi}\frac{24\,m}{L^3}\left[-\operatorname{acoth}\left(2\frac{r}{L}\right)+\frac{L}{2r}+\frac{L^3}{8r\left(r^2-\frac{L^2}{4}\right)}\right]$$
$$= \frac{1}{4\pi}\frac{m}{r^3}\left[2+\frac{9}{20}\frac{L^2}{r^2}+\frac{3}{14}\frac{L^4}{r^4}+\ldots\right].$$

The on-axis fields of the point dipole (magnetized sphere), magnetized splinter, and physical dipole are plotted in Fig. 2. The fields are normalized to the strength of the point dipole being 2 at r = 1, and the distances are normalized to L = 1. Both the magnetized splinter and physical dipole are somewhat stronger than the point dipole, which could be misinterpreted if using the point dipole approximation by predicting the objects to be somewhat closer than they actually are. Again, the magnetized splinter is intermediate between the sphere and the physical dipole.

Polarizability Tensor of the Physical Dipole

Like for the magnetized splinter, the dipole moment $\vec{m}$ is given and the internal fields are not of interest, one reason being the vanishing volume. However, the polarizability $\vec{m}$ is still defined via $\vec{m} = \boldsymbol{\alpha}\vec{H}_a$. If desired, the physical dipole can be modeled as having a very small $V \ll L^3$ of magnetic material with very large $\chi \gg 1$. Then for the physical dipole, in that limit $\boldsymbol{\alpha}$ is diagonal with

$$\alpha_{xx} = \alpha_{yy} = 0,\ \alpha_{zz} = V\chi.$$

Note $\boldsymbol{\alpha}$ is not invertible for the physical dipole, and the demagnetization factors do not exist.

The Multipole Expansion of the Physical Dipole

For $r > \frac{L}{2}$, the multipole expansion of the external potential of the physical dipole with $\hat{m} = \hat{z}$ is:

$$\Phi = \frac{m}{r^2}\sum_{k=0}^{\infty}\left(\frac{L}{2r}\right)^{2k} P_{2k+1}(\cos\theta),$$

where the argument of the Legendre polynomial is $\cos\theta = \frac{z}{r}$. Only the odd Legendre polynomial terms survive because of the reflection antisymmetry of the physical dipole on the z-axis. The simplicity of the multipole expansion of the physical dipole is striking,

especially compared with the multipole expansions of the spheroids and other models.

Conclusions and Recommendations

The magnetized splinter is the extreme prolate spheroid, the spheroid that is most different from the sphere. Hence, it could be used as an end-member in model selection. For instance, if the point dipole is the first model tried in a sequence of model fitting, and it does not fit well, then the external field of the magnetized splinter could be the next model to try to fit. As an example, use of near-field data for the point dipole model could produce an inconsistent estimate of the location, while the magnetized splinter model may be more consistent. However, as shown herein, the external field of the physical dipole is actually somewhat more extreme than the magnetized splinter, in the sense that the field strength of the magnetized splinter is always between the physical dipole and the point dipole. Thus, the physical dipole is a better end-member for model selection.

Moreover, numerically the expressions for the physical dipole are more convenient and better behaved. As an example, the physical dipole converges directly to the point dipole in the limit as $L \rightarrow 0$, but similar analyses in that limit for the magnetized splinter require more work to take care of the various divergent quantities. Such divergences and the resulting instability can be important in numerical model fitting and parameter estimation. Also, because the point dipole is simply the direct limit of small L, the point dipole does not need separate fitting. Indeed, some texts define the point dipole as the small L limit of the physical dipole (Shadowitz, 1975). The multipole expansion of the physical dipole is also much more convenient and better behaved than the multipoles for the magnetized splinter.

Although the physical dipole model has not been applied before for parameter estimation of magnetic objects such as UXO in the field, it is both analytically and numerically simpler than other models such as prolate spheroids. It has only the one extra parameter L than the point dipole model, and its shape orientation is not fit separately from its dipole moment so direction ambiguity is minimized. These considerations lead to the recommendation that, in order to quantify its applicability, the physical dipole model should be applied to some existing data sets.

The polarizability tensor is better behaved and better defined than the various demagnetization tensors. The polarizability also provides a simple way to estimate the outer volume of magnetic material. Hence, in the context of UXO detection, more use should be made of the magnetostatic polarizability of objects.

Acknowledgments

This research was supported by the U.S. Army Engineer Environmental Quality and Installations Program at the U.S. Army Engineer Research and Development Center (ERDC), Vicksburg, MS. The use of the extensive U.S. Army Environmental Quality Technology (EQT) Research compendium of UXO reports and articles, available through the EQT Program Management Office at ERDC, is gratefully acknowledged.

References

Altshuler, T., 1996, Shape and orientation effects on magnetic signature prediction for unexploded ordnance: *in* Proceedings 1996 UXO Forum, Williamsburg, VA, 282–291.

Altshuler, T., Andrews, A., and Sparrow, D., 1997, Mine and UXO detection: measures of performance and their implication in real-world scenarios: Proceedings of SPIE, **3079**, 281–292.

Barrow, B., DiMarco, R., Khadr, N., and Nelson, H., 1997, Processing and analysis of UXO signatures measured with MTADS: *in* Proceedings 1997 UXO Forum, Nashville, TN, 8–18.

Bell, T., and Barrow, B., 1997, Model-based processing helps new UXO sensors separate ordnance from scrap: Ordnance and Explosives Environment Newsletter, **4**, 3.

Billings, S., Pasion, L., and Oldenburg, D., 2002. Discrimination and identification of UXO by geophysical inversion of total-field magnetic data, ERDC/GSL TR-02-16: U.S. Army Engineer Research and Development Center, Vicksburg, MS.

Billings, S., 2004, Discrimination and classification of buried unexploded ordnance using magnetometry: IEEE Transactions on Geoscience and Remote Sensing, **42**, 1241–1251.

Billings, S., Pasion, C., Walker, S., and Beran, L., 2006, Magnetic models of unexploded ordnance: IEEE Transactions on Geoscience and Remote Sensing, **44**, 2115–2124.

Billings, S., Pasion, L., Lhomme, N., and Song, P., 2008. UXO characterization: comparing cued surveying to standard detection and discrimination approaches: report 6 of 9 - advanced electromagnetic and magnetic methods for discrimination of unexploded ordnance, ERDC/EL TR-08-37: U.S. Army Engineer Research and Development Center, Vicksburg, MS.

Billings, S., 2009, Field measurements of induced and remanent moments of unexploded ordnance and shrapnel: IEEE Transactions on Geoscience and Remote Sensing, **47**, 815–827.

Brown, W., 1962. Magnetostatic principles in ferromagnetism, North-Holland Publishing Company, Amsterdam.

Butler, D., Cespedes, E., Cox, C., and Wolfe, P., 1998. Multisensor methods for buried unexploded ordnance detection, discrimination, and identification, Technical

report SERDP-98-10: U.S. Army Engineer Waterways Experiment Station, Vicksburg, MS.

Butler, D., 2001, Potential fields methods for location of unexploded ordnance: The Leading Edge, **20**, 890–895.

Butler, D., Wolfe, P., and Hansen, R., 2001, Analytical modeling of magnetic and gravity signatures of unexploded ordnance: Journal of Environmental and Engineering Geophysics, **6**, 33–46.

Butler, D., Young, R., and Vieth, W., 2002, UXO-101: an introduction to unexploded ordnance, Short course: *in* Proceedings: 15th Symposium on the Application of Geophysics to Engineering and Environmental Problems, Denver, CO.

Butler, D., 2003, Implications of magnetic backgrounds for unexploded ordnance detection: Journal of Applied Geophysics, **54**, 111–125.

Butler, D., Pasion, L., Billings, S., Oldenburg, D., and Yule, D., 2003, Model-based inversion for enhanced UXO detection and discrimination: Proceedings of SPIE, **5089**, 958–969.

Butler, D., Yule, D., and Bennett, H., 2004, Employing multiple geophysical sensor systems to enhance buried UXO target recognition capability: *in* Proceedings of 24th U.S. Army Science Conference, Orlando, FL.

Cape, J., and Zimmerman, J., 1967, Magnetization of ellipsoidal superconductors: Physical Review, **153**, 416–421.

Chen, D.-X., Brug, J., and Goldfarb, R., 1991, Demagnetizing factors for cylinders: IEEE Transactions on Magnetics, **27**, 3601–3619.

Chen, D.-X., Pardo, E., and Sanchez, A., 2005, Demagnetizing factors for rectangular prisms: IEEE Transactions on Magnetics, **41**, 2077–2088.

Dirac, P., 1931, Quantized singularities in the electromagnetic field: Proceedings of the Royal Society, **A133**, 60–72.

DeProspo, D., and DiMarco, R., 1996, Automatic detection and characterization of magnetic anomalies in total field magnetometer data: *in* Proceedings 1996 UXO Forum, Williamsburg, VA, 301–307.

Frumkis, L., and Kaplan, B.-Z., 1999, Spherical and spheroidal shells as models in magnetic detection: IEEE Transactions on Magnetics, **35**, 4151–4158.

Gasperikova, E., Smith, J., Morrison, H., and Becker, A., 2007, Berkeley UXO discriminator (BUD): *in* Proceedings: 20th Symposium on the Application of Geophysics to Environmental and Engineering Problems, 1049–1055.

Gerovska, D., Arauzo-Bravo, M., and Stavrev, P., 2004, Determination of the parameters of compact ferrometallic objects with transforms of magnitude magnetic anomalies: Journal of Applied Geophysics, **55**, 173–186.

Gorkunov, E., Zakharov, V., Zembekov, N., Ul'yanov, A., and Chulkina, A., 2005, Demagnetizing factors of ferromagnetic bars upon magnet saturation: Russian Journal of Nondestructive Testing, **41**, 80–85.

Herrera-May, A., Aguilera-Cortés, L., García-Ramírez, P., and Manjarrez, E., 2009, Resonant magnetic field sensors based on MEMS technology: Sensors, **9**, 7785–7813.

Jackson, J., 1975. Classical electrodynamics, 2nd ed., John Wiley & Sons, Inc., New York.

Kellogg, O., 1954. Foundations of potential theory, Dover, New York.

Lieblich, D., 2004. Physics of scrap discrimination, Final report SERDP SEED UX-1356, Strategic Environmental Research and Development Program, Arlington, VA.

Mahan, G., and Subbaswamy, K., 1990. Local density theory of polarizability, Plenum Press, New York.

Maxwell, J., 1891. A treatise on electricity and magnetism, 3rd ed., Clarendon Press, Oxford.

McFee, J., and Das, Y., 1986, Fast nonrecursive method for estimating location and dipole moment components of a static magnetic dipole: IEEE Transactions on Geoscience and Remote Sensing, **24**, 663–673.

McFee, J., 1989. Electromagnetic remote sensing: low frequency electromagnetics, DRES-SP-124, Defence Research Establishment Suffield, Canada.

Moskowitz, R., and Della Torre, E., 1966, Theoretical aspects of demagnetization tensors: IEEE Transactions on Magnetics, **2**, 739–744.

Moskowitz, R., Della Torre, E., and Chen, R., 1966, Tabulation of magnetometric demagnetization factors for regular polygonal cylinders: Proceedings of the IEEE, **54**, 1211.

Nelson, H., and McDonald, J., 1998, Analysis of magnetometer and EMI data for the MTADS program: Proceedings of the 7th IEEE International Conference on Fuzzy Systems, 241–245.

Newell, A., Williams, W., and Dunlop, D., 1993, A generalization of the demagnetizing tensor for nonuniform magnetization: Journal of Geophysical Research, **98**(B6) 9551–9555.

Norton, S., Won, I., and Cespedes, E., 2001, Spectral identification of buried unexploded ordnance from low-frequency electromagnetic data: Subsurface Sensing Technologies and Applications, **2**, 177–189.

Osborn, J., 1945, Demagnetizing factors of the general ellipsoid: Physical Review, **67**, 351–357.

Pardo, E., Chen, D.-X., and Sanchez, A., 2004, Demagnetizing factors for square bars: IEEE Transactions on Magnetics, **40**, 1491–1498.

Pennella, J., 1982. Magnetometer techniques in the detection of projectiles, NAVEODTECHCEN technical report TR-239: Naval Explosive Ordnance Disposal Technology Center, Indian Head, MD.

Reitz, J., and Milford, M., 1962. Foundations of electromagnetic theory: Addison-Wesley, Reading, MA.

Rene, R., Kim, K., and Park, C., 2008, Intra-inversion filtering for overlapping magnetic fields of unexploded ordnance (UXO), clutter and geology: Journal of Environmental and Engineering Geophysics, **13**, 147–164.

Schabes, M., and Aharoni, A., 1987, Magnetostatic interaction fields for a 3-dimensional array of ferromagnetic cubes: IEEE Transactions on Magnetics, **23**, 3882–3888.

Schlomann, E., 1962, A sum rule concerning the inhomogeneous demagnetizing field in nonellipsoidal samples: Journal of Applied Physics, **33**, 2825–2826.

Shadowitz, A., 1975. The electromagnetic field: McGraw-Hill Book Company, New York.

Shubitidze, F., Karkashadze, D., Barrowes, B., and O'Neill, K., 2007, An analytical expression for estimating a buried object's location, orientation and magnetic polarization to support UXO discrimination: *in* Proceedings XIIth International Seminar/Workshop on Direct and Inverse Problems of Electromagnetic and Acoustic Wave Theory (DIPED-2007), Lviv, Ukraine.

Smith, J., and Morrison, H., 2004, Estimating equivalent dipole polarizabilities for the inductive response of isolated conductive bodies: IEEE Transactions on Geoscience and Remote Sensing, **42**, 1208–1214.

Stoner, E., 1945, The demagnetizing factors for ellipsoids: Philosophical Magazine, **36**, 803–821.

Sun, K., O'Neill, K., Barrowes, B., Fernandez, J., Shubitidze, F., Shamatava, I., and Paulsen, K., 2006, Dumbbell dipole model and its application in UXO discrimination: Proceedings of SPIE, **6217**, 601–612.

Tejedor, M., Rubio, H., Elbaile, L., and Iglesias, R., 1995, External fields created by uniformly magnetized ellipsoids and spheroids: IEEE Transactions on Magnetics, **31**, 830–836.

Won, I., Keiswetter, D., and Bell, T., 2001, Electromagnetic induction spectroscopy for clearing landmines: IEEE Transactions on Geoscience and Remote Sensing, **39**, 703–709.

Zijlstra, H., 1967. Experimental methods in magnetism: North-Holland Publishing Company, Amsterdam.